Journal of Innovative Optical Health Sciences
Vol. 9, No. 4 (2016) 1642004 (11 pages)

DOI: 10.1142/S1793545816420049

The morphological changes in the internal organs of laboratory animals after prolonged oral administration of gold nanoparticles

Alla B. Bucharskaya[*,‖], Galina N. Maslyakova[*], Svetlana S. Pakhomy[*], Olga V. Zlobina[*], Irina O. Bugaeva[*], Nikita A. Navolokin[*], Boris N. Khlebtsov[†], Vladimir A. Bogatyrev[†], Nikolai G. Khlebtsov[†,‡] and Valery V. Tuchin[‡,§,¶]

[*]*Saratov State Medical University n.a.V.I. Razumovsky*
410012 Saratov, Russia

[†]*Institute of Biochemistry and Physiology of Plants and Microorganisms RAS*
410049 Saratov, Russia

[‡]*Research-Educational Institute of Optics and Biophotonics*
Saratov National Research State University
410012 Saratov, Russia

[§]*Institute of Precision Mechanics and Control RAS*
410028 Saratov, Russia

[¶]*Interdisciplinary Laboratory of Biophotonics*
Tomsk National Research State University, 634050 Tomsk, Russia
[‖]*allaalla_72@mail.ru*

Received 20 November 2015
Accepted 10 May 2016
Published 20 June 2016

Recently gold nanoparticles (GNPs) have been actively studied as photothermal converters, drug carriers, and imaging agents in a wide range of applications in cancer diagnosis and therapy. The prolonged peroral administration of GNPs in a range of sizes was performed to investigate the morphological changes and their reversibility in the internal organs of laboratory animals. In this study, GNPs with average diameters of 2 nm, 15 nm and 50 nm were administered during 30 days, and the reversibility of morphological changes was investigated 14 days after administration. After the prolonged administration of GNPs, the severity of morphological changes in the liver, kidney, spleen and lymph nodes depended on the nanoparticle size. Specifically, 50 nm nanoparticles caused the most pronounced dystrophic and necrobiotic effects, whereas the smallest 2 nm nanoparticles caused proliferative changes. Most importantly, the development of pathological processes was reversible, as evidenced by the gradual restoration of the organ structure at 14 days after the end of GNPs administration.

[‖]Corresponding author.

Keywords: Gold nanoparticles; prolonged peroral administration; morphological changes; reversibility.

1. Introduction

Over the past two decades, active development and applications of inorganic nanomaterials[1] and gold nanoparticles (GNPs)[2] in particular have been observed in various fields of nanomedicine for diagnostic and therapeutic purposes.[3–6] Due to the small size and plasmon-resonant properties of GNPs, they can act as local heaters and light-scattering or optoacoustic labels, while due to surface functionalization they can be used as targeted carriers of targeting molecules, drugs, peptides, DNA and RNA for applications such as biological sensing, imaging, and photodynamic, photothermal and genomic therapies.[7,8] Two drugs for intravenous administration — AurImmune™ and AuroLase™ — have already passed the clinical trials for rheumatoid arthritis.[9,10] Extensive material has also published on the clinical trials of the gold-based drug Aurasol® in tablet form for the treatment of severe rheumatoid arthritis.[11]

Toxicity concerns arose almost simultaneously with the beginning of applications of GNPs and other nanomaterials to nanomedicine. It is currently believed that the biological and toxic effects of nanoparticles depend on several critical parameters such as the particle size and shape, the nature of surface functionalization, the dose and the route of administration.[6,12–14] Although several reports on the possible genotoxicity of small GNPs have been published,[15–17] other authors did not confirm these findings.[18] However, there is a satisfactory consensus on significant accumulation of GNPs in the liver and spleen of animals with very slow clearance kinetics.[6] Moreover, first reports have been published on the penetration of GNPs through the placental barrier in pregnant mice[19,20] and rats.[21] It should be emphasized that the toxicity of GNPs can be determined by various surface stabilizing agents rather than the gold nanomaterial *per se*. For instance, cetyltrimethylammonium bromide (CTAB) is a typical surface stabilizer for as-prepared gold nanorods, and CTAB is a known toxic surfactant in its free state.[13]

Numerous reports on the biodistribution, toxicity[5,6,14] and cellular uptake of GNPs[22] have been published over the past decade. There has been wide variation in experimental design, including the size and shape of particles, methods of functionalization, types of animals, dose and route of administration of the particles. Accordingly, wide variation in the data and findings was observed in the levels and kinetics of the biodistribution and toxicity assessments. Regarding the administration route, oral administration may cause some effects on the digestive system, while tail vein injection mainly acts on the blood and related organs. Indeed, Hillyer and Albrecht[23] showed that the oral administration of GNPs could result in strong gastrointestinal persorption effects. It has also been shown that the oral delivery of nanoparticles may affect the mucosa due to the morphological and physiological absorption barriers in the gastrointestinal tract.[24] Therefore, gastrointestinal reaction and absorption would play an important role in the oral administration of GNPs. Despite numerous reports on the biodistribution and toxicity of GNPs after intravenous administration, the current understanding of morphological effects caused by GNPs after prolonged oral administration and data on possible reversibility of morphological changes in organs remain limited.

This study is aimed at a comparative evaluation of morphological changes in the internal organs in rats and the reversibility of those changes after prolonged oral administration of GNPs with different average sizes.

2. Materials and Methods

GNPs with average diameters of 2 nm, 15 nm and 50 nm and a mass-volume concentration of 57 μg/mL were synthesized as previously described.[25] In particular, 15 nm and 50 nm GNPs were synthesized by the Frens method,[26] and the smallest 2 nm GNPs were obtained by the Duff method.[27] The corresponding particle number concentrations are 8.8×10^{13}, 1.7×10^{12}, and 4.5×10^{10} particles/mL, respectively. The average size of the GNPs was determined from electron microscopic images obtained using a Libra-120 microscope (Carl Zeiss,

Germany) in Centre of Collective Use of Institute of Biochemistry and Physiology of Plants and Microorganisms RAS (Russia).

For increased biocompatibility, 15 nm and 50 nm GNPs were conjugated with thiolated polyethylene glycol mPEG-SH ($M_w = 5000$, Nektar Therapeutics) as described previously.[25] The smallest 2 nm GNPs were used as prepared. The GNP-mPEG conjugates were formed by the covalent binding of thiol groups to the surface of GNPs. The resulting conjugates were washed twice by centrifugation to remove excess reaction products and resuspended in 0.9% sodium chloride solution.

The experimental study was conducted in Centre of Collective Use of Saratov State Medical University (Russia). The experiment was performed using 40 healthy adult albino male rats weighing 180–220 g. The rats were kept under a constant 12 h light-dark cycle at 22–25°C with standard chow and water provided ad libitum. The experiment was divided into two series. The first series included the study of morphological changes in the organs during a 30-day oral administration of GNPs of different sizes. Three experimental groups and a control group of animals were formed randomly (10 animals in each group). 30 days after, half of the animals in each group were deduced from the experiment. 14 days after the end of GNP administration, we examined the reversibility of the detected changes in remaining animals. For morphological examination, the organ specimens of rats (liver, kidney, spleen, lymph nodes) were fixed in 10% formalin solution, then subjected to a standard alcohol and acetone wiring and embedded in paraffin. After sample dewaxing, 5–7 micron thick sections were stained with hematoxylin and eosin (H-E). Morphometric analysis of the histological preparations was conducted in 30 fields of view at magnification 774.0× using the digital image analysis system Mikrovizor medical μVizo-103 (LOMO, Russia).

Counting of cell elements of mesenteric lymph nodes were carried out in the various functional areas of the lymph node by the standard method with magnification 1000× using morphometric software Image Analyzer in 10 fields of view on the conventional unit area (6400 μm^2). Digital camera SCOPETEK DCM (Hangzhou Scopetek Opto-Electric Co., China) is used to capture histopathological images. The classification of analyzed cell elements was conducted according to required criteria and reporting. Analysis of results was displayed in the form of histograms, charts and tables.

The Perls reaction[28] was used for the differential diagnosis of hemosiderin and GNP clusters. The dark-field microscopy was conducted in Centre of Collective Use of Institute of Biochemistry and Physiology of Plants and Microorganisms RAS (Russia). Leica DM 2500 microscope with a special attachment that permits lateral illumination at 630.0× and 1500.0× magnifications was used to identify clusters of GNPs in tissue sections.

The reaction with methyl green pyronin by Brachet[28] was used to identify and count the number of plasma cells in the lymph nodes.

The immunohistochemical method was performed using rabbit polyclonal antibodies (Anti-Ki67, Abcam, United Kingdom) to study the proliferative activity of hepatocytes. A REVEAL — Biotin-Free Polyvalent DAB system (Spring Bioscience, USA) was used for visualization of the immunohistochemical reactions.

The experimental data were analyzed using a statistical software package application, STATISTICA 10.0 (StatSoft Inc., USA). Preliminary statistical data processing was performed by the Kolmogorov–Smirnov test to verify compliance of distribution forms to normal, and the equality of the population variance was determined using the Fisher F-test. The null hypothesis was rejected when $p < 0.05$. The arithmetic mean (M) and the standard deviation (σ) were calculated for each index. The differences between the samples were assessed using Student's t-test.

3. Research Involving Animals

Two series of animal experiments were conducted according to the University's Animal Ethics Committee and the relevant national agency regulating experiments in animals. The international guiding principles for biomedical research involving animals of the Council for the International Organization of Medical Sciences and International Council for Laboratory Animal Science (CIOMS and ICLAS) were followed during the animal experiments.[29]

4. Results and Discussion

In the histological study of stomach mucosa sections, morphological changes were unidirectional in

nature in the animal groups with of administration 2 nm, 15 nm and 50 nm GNPs, and gross defects in the structure were not detected. The mucosa was maintained in all experimental groups. The surface of the gastric mucosa was lined with a single layer of prismatic epithelium. The gastric pits had normal depth and were lined by columnar epithelium. The mucosal infiltration by eosinophils was noted in all experimental groups. The submucosa was not changed and consisted of loose connective tissue with blood vessels. The stomach glands were located in the lamina propria of the mucosa, and thin layers of loose fibrous connective tissue lay between the glands. Vessels of the mucosa and submucosa had normal structure, although there was sometimes a slight congestion.

14 days after 30-day administration of GNPs the gastric mucosa exhibited normal histological structure in all experimental groups, and no accumulation of eosinophils and conglomerates of GNPs was revealed.

The most pronounced morphological changes were found in the liver, most likely due to the detoxification function of the organ. It should be noted that conglomerates of GNPs were absent in the liver in all cases. We recorded only indirect signs of their presence in the form of dystrophic and necrotic changes of the parenchyma and activation of the monocyte-macrophage system.

The administration of 2 nm and 50 nm GNPs caused the most pronounced morphological changes in the liver: the absence of a beam structure and marked vacuolar degeneration of hepatocytes were revealed compared with control (see Figs. 1(a) and 1(b)). The beam structure of hepatocytes was preserved in the group that received 15 nm GNPs, but moderate degeneration of the parenchyma was noted (Fig. 1(c)).

To study the influence of GNPs on the liver morphology, morphometric analysis was conducted using such indicators as the parenchyma normalization coefficient (PNC) and counting of the number of lymphocytes, Kupffer cells, Ito cells and binucleated hepatocytes. The PNC was counted as the ratio of the number of normal hepatocytes to hepatocytes in a state of degeneration and necrosis. PNC is an important criterion in the morphological assessment of the liver structure because it allows to estimate the intensity of dystrophic and necrobiotic changes in the liver.[30]

Morphometric analysis revealed significant reductions in the amount of unaltered hepatocytes and the PNC after 30-day peroral administration of GNPs (Table 1). The minimum value of the PNC (0.09 ± 0.03) was obtained after prolonged peroral administration of 50 nm GNPs. In all experimental groups, the numbers of lymphocytes and of Kupffer and Ito cells in the liver were higher than the control values.

The partial restoration of the morphological structure of organs in all groups was noted in the reversibility study: the severity of degeneration was reduced 14 days after prolonged peroral administration of GNPs (see Fig. 3(a)). According to morphometric analysis at 14th day after GNP administration, PNC increased more than six times in all test groups but remained below the control values (Table 1). The changes in the monocyte-macrophageal system had a size-dependent character. Further increase in lymphocytes and Kupffer cells were recorded in the group of animals with administration of 2 nm GNPs, whereas a decrease in

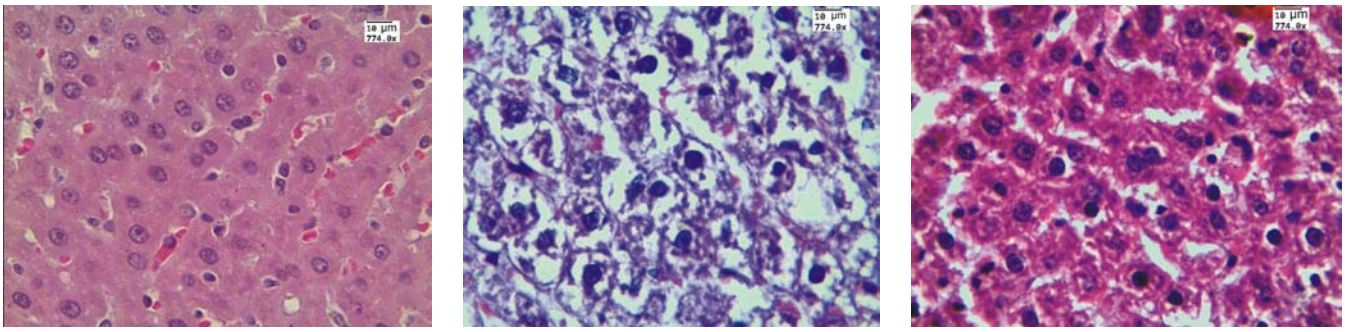

(a) (b) (c)

Fig. 1. (a) Liver in control group of animals. (b) Expressed degeneration and necrosis of hepatocytes after 30-day administration of 50 nm GNPs. (c) Dystrophic changes in hepatocytes after 30-day administration of 15 nm GNPs. H-E staining, magnification 774.0×.

Table 1. Morphological changes in liver at 30-day oral administration of GNPs and 14 days after.

		Groups of animals					
		2 nm GNPs		15 nm GNPs		50 nm GNPs	
Indicators ($M \pm \sigma$) in 30 fields of view	Control group	30-day adm.	14 days after	30-day adm.	14 days after	30-day adm.	14 days after
Degree of severity of hepatocyte dystrophy	–	+++	+	++	+	+++	+
Degree of plethora severity	+/++	+	+++	++	++/+++	++/+++	++/+++
Blood separation	–	+/–	+	–	+	–	+/–
Number of hepatocytes with signs of dystrophy	37.2 ± 4.1	167 ± 12*	59 ± 8.9*	149 ± 11*	51.8 ± 5.6*	205 ± 15*	62.3 ± 7.9*
Number of normal hepatocytes	432 ± 25	33.8 ± 9.4*	365 ± 14*	122 ± 33*	376 ± 11*	20.6 ± 6.3*	380 ± 15*
Number of hepatocytes with necrosis signs	–	79.7 ± 8.1*	28.5 ± 3.8	59.7 ± 8.9*	26.5 ± 4.9	96.8 ± 8.5*	51.2 ± 5.9
Parenchyma normalization coefficient (PNC)	11.7 ± 1.7	0.2 ± 0.06*	6.1 ± 0.5*	0.82 ± 0.43*	7.65 ± 0.7*	0.09 ± 0.03*	6.2 ± 0.56*
Number of lymphocytes	17.6 ± 4.2	32.5 ± 7.6	52.2 ± 6.4*	36.3 ± 11.8*	30.6 ± 6.7*	39.6 ± 5.1	27.6 ± 6.0*
Number of Kupffer and Ito cells	8.5 ± 2.3	22.6 ± 4.6	27.8 ± 6.5*	23.1 ± 3.9*	15.1 ± 5.6*	26.9 ± 4.1*	14.6 ± 3.3*
Number of binucleated hepatocytes	5.6 ± 1.5	5.1 ± 1.2	16.8 ± 3.3*	6.9 ± 1.8	18.5 ± 1.7*	6.41 ± 1.8	15.5 ± 2.5*

Note: M is arithmetic mean (M) and σ is the standard deviation; * is P calculated relative to the control group ($P < 0.05$).

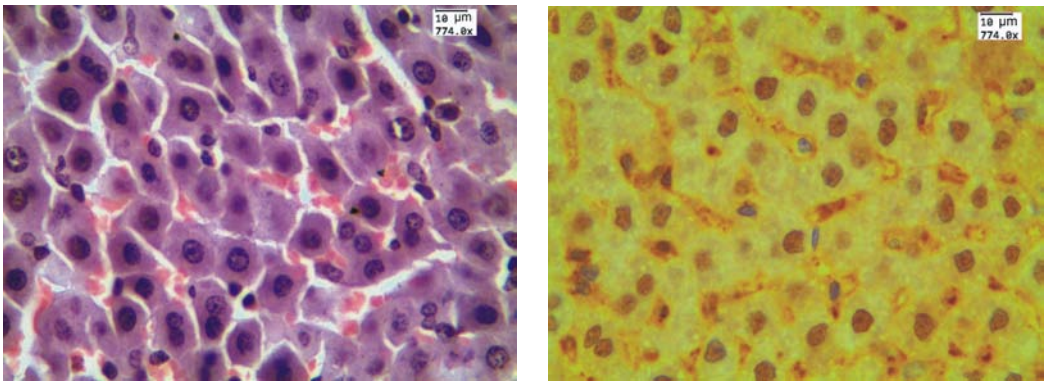

(a) (b)

Fig. 2. (a) The signs of degeneration of hepatocytes 14 days after 15 nm GNP administration. H-E staining, magnification 774.0× (b) Marked expression of nuclear antigen Ki-67 protein in hepatocytes after 30-day administration of 15 nm GNPs. Immunohistochemical staining, magnification 774.0×.

cell numbers to the initial value was noted 14 days after prolonged administration of 15 nm and 50 nm GNPs. The number of binucleated hepatocytes increased in all experimental groups.

By immunohistochemical study, after 30-days administration of GNPs the significant differences was noted in all test groups compared to control values (see Fig. 2(b)). The marked positive reaction with the marker Ki-67 was observed in all test groups, indicating a high proliferative activity of hepatocytes — up to 70–80% cells with positive expression (the control value was 4.1%). In the reversibility study, the number of hepatocytes with positive expression had decreased in all test groups to 30–40% cells with Ki-67 positive expression at 14th day after the 30-day administration of GNPs.

We regarded the increasing number of binucleated hepatocytes as a development of regenerative processes, contributing to the restoration of liver tissue by increasing the number of hepatocytes. We agree with the authors[31] that the increase in the number of binucleated hepatocytes indicates increased protein-synthetic function of the liver, which can be regarded as a single compensatory-adaptive mechanism aimed at normalizing the structure and functions of the organ.

The morphological changes in the kidney presented mostly moderate vascular hyperemia of the cortex, with degenerative and necrotic changes in the epithelium of the convoluted tubules of mild to moderate severity. The most pronounced morphological changes (expressed hyperemia of glomerular capillaries, marked degeneration and fragmentation of the cytoplasm from the epithelium of the convoluted tubules, necrosis of epithelial cells) were found in the group administered 50 nm GNPs (see Fig. 3). Dystrophy of the epithelium of the convoluted tubules was noted in the animal groups with 30-day administration of 2 nm and 15 nm GNPs. In the study of the reversibility of morphological changes in the kidneys, the severity of degeneration of the epithelium of convoluted tubules decreased in the groups of animals administered 2 nm and 15 nm GNPs and remained severe in the group administered 50 nm GNPs. It should be noted that GNP conglomerates in the kidneys were not found by dark-field microscopy.

In the spleen in all groups, the boundary between the red and white pulp was not clearly distinct, lymphoid follicles were significantly increased in size, containing bright germinative centers represented by large blast cells. In the study of reversibility in the spleen, decreased size of lymphoid follicles was observed upon administration of 2 nm and 15 nm GNPs, and the germinative centers were not noted. In the group of animals administered 50 nm GNPs, the sizes of the lymphoid follicles increased, and the bright germinative centers remained, represented by large blast cells.

In all experimental groups of animals, the accumulation of black pellets was noted in the red pulp of the spleen. Using the Perls reaction, the granules (hemosiderin) were stained in blue while the other part (GNPs) remained black (see Fig. 4(a)). The unpainted granules showed a red color in dark-field microscopy of preparations stained by Perls (see Fig. 4(b)).

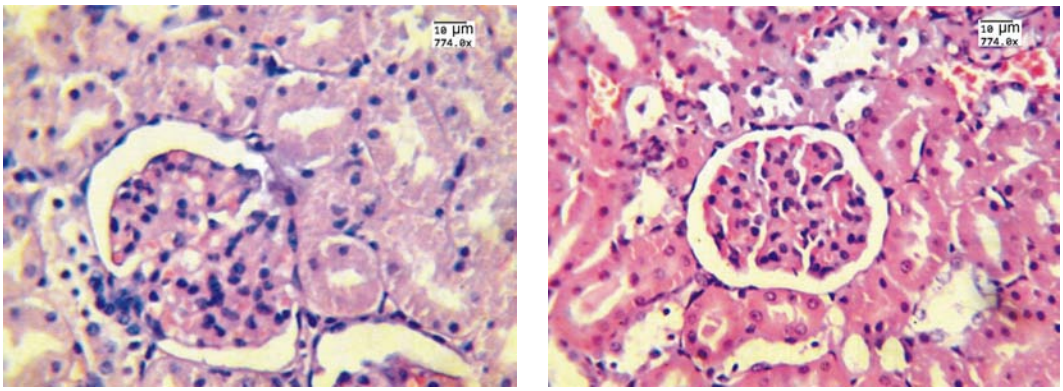

(a) (b)

Fig. 3. (a) Severe degeneration and necrosis of the epithelium of the convoluted tubules of kidney after 30-day administration of 50 nm GNPs. (b) Dystrophy of the epithelium of convoluted tubules of kidney after 30-day administration of 15 nm GNPs. H-E staining, magnification 774.0×.

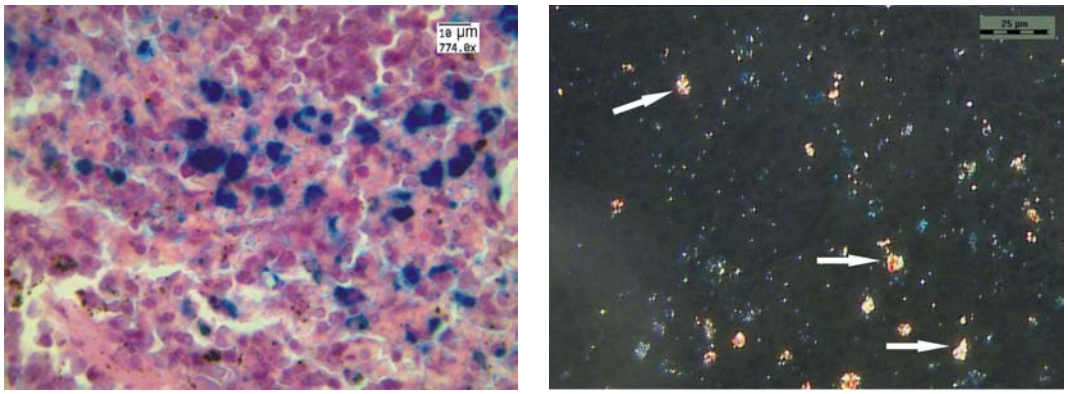

(a) (b)

Fig. 4. (a) Two types of particles in the spleen: granules of hemosiderin are blue, while conglomerates of GNPs are black. Staining by Perls, magnification 774.0× (b) Glow of GNPs due to intensive light scattering. The arrows demonstrate conglomerates of GNPs. Dark-field microscopy, magnification 630.0×.

In the mesenteric lymph nodes, after 30-days administration of GNPs the changes in cellular composition were observed in all experimental groups. In groups administered 2 and 50 nm GNPs, the changes were found in all functional areas of lymph nodes: increased lymphoid follicles with germinative centers representing immunoblasts, macrophages and mitotic figures were noted in the cortex (Table 2); the medulla cords increased due to increased number of plasma cells; increased number of small, middle and large lymphocytes was revealed in the paracortical zone. In the group administered 15 nm GNPs more pronounced changes were found in the paracortical area than in the areas of lymphoid follicles and medulla cords.

Under dark-field microscopy, conjugates of GNPs were found in the cytoplasm of macrophages (see Fig. 5) and lymphocytes predominantly in the mantle zone of the lymphoid follicles and in medulla cords in the groups administered 15 nm and 50 nm GNPs. Extracellular accumulation of GNPs was detected in medulla sinuses. It should be noted that 2 nm GNPs were not recorded by available methods in any zones of the lymph nodes.

In the reversibility study, after cessation of administration of 15 nm and 50 nm GNPs, the number of cell elements of lymph node corresponded to the control values. Only in the group administered 2 nm GNPs, the changes in cellular composition persisted in all functional areas of the lymph nodes.

Table 2. The morphological changes in mesenteric lymph nodes at 30 days administration of GNPs and 14 after.

			Experimental groups with GNPs administration					
			2 nm		15 nm		50 nm	
Zones of lymphatic nodes	The number of cells (within area of 6400 μm^2)	Control group	30-day adm.	14 days after	30-day adm.	14 days after	30-day adm.	14 days after
Lymph follicles	Small lymphocytes	64.2 ± 3.1	73.2 ± 1.1*	72.6 ± 1.8*	68.7 ± 1.4	67.5 ± 1.3	76.2 ± 0.4*	69.4 ± 1.6
	Middle lymphocytes	18.2 ± 1.4	30.1 ± 1.8*	26.2 ± 0.9*	30.2 ± 0.6*	20.8 ± 3.1	25.7 ± 1.3*	30.4 ± 0.9*
	Large lymphocytes	0	1.4 ± 0.2*	1.2 ± 0.1*	10.4 ± 0.6*	1.9 ± 0.6*	10.3 ± 0.6*	6.7 ± 0.4*
	Immunoblasts	2.5 ± 0.3	4.2 ± 0.9*	3.1 ± 0.4	3.1 ± 0.6	3.4 ± 0.4*	2.7 ± 0.2	2.2 ± 0.1
	Plasmocytes	0	0	0	0	0	0	0
	Mastocytes	0	0	0	0	0	0	0
	Mitotic figures	0.2 ± 0.1	1.2 ± 0.1*	0.8 ± 0.1*	1.0 ± 0.4*	0.3 ± 0.1	0.9 ± 0.1*	0.6 ± 0.1*
Paracortical zone	Small lymphocytes	60.1 ± 3.2	80.1 ± 1.6*	74.2 ± 1.3*	70.6 ± 2.1*	61.8 ± 2.4	70.3 ± 0.8*	74.3 ± 2.2*
	Middle lymphocytes	12.1 ± 1.1	19.6 ± 1.4*	16.7 ± 0.5*	20.4 ± 1.6*	13.7 ± 2.6	26.7 ± 1.4*	28.3 ± 0.4*
	Large lymphocytes	0.8 ± 0.1	2.0 ± 0.4*	1.8 ± 0.2*	1.4 ± 0.7*	1.1 ± 0.4	1.8 ± 0.2*	1.0 ± 0.4
	Immunoblasts	0	0.8 ± 0.1	0.9 ± 0.2	3.0 ± 0.4	2.1 ± 0.2	1.8 ± 0.5*	2.0 ± 0.2*
	Plasmocytes	0.7 ± 0.1	1.6 ± 0.2*	1.1 ± 0.09	16.4 ± 0.2*	0.5 ± 0.1	1.0 ± 0.1	0.8 ± 0.1
	Mastocytes	0	0	0	0	0	0	0
	Mitotic figures	0.8 ± 0.2	1.4 ± 0.1*	1.1 ± 0.2	1.5 ± 0.2*	0.8 ± 0.1	1.0 ± 0.2	1.3 ± 0.1*
Medulla cords	Small lymphocytes	20.2 ± 1.3	28.6 ± 2.2*	26.1 ± 2.2*	24.8 ± 1.9*	20.5 ± 1.8	24.7 ± 1.4	19.7 ± 0.8
	Middle lymphocytes	10.2 ± 1.7	19.2 ± 0.8*	14.3 ± 0.4	16.8 ± 0.9*	11.1 ± 1.1	16.2 ± 1.6*	12.6 ± 1.2
	Large lymphocytes	10.2 ± 1.7	16.7 ± 0.8*	14.3 ± 0.8*	10.8 ± 0.7	9.2 ± 0.6	8.2 ± 0.6*	10.4 ± 0.1
	Immunoblasts	2.3 ± 0.3	2.5 ± 0.5	2.3 ± 0.4	4.9 ± 0.5*	3.3 ± 0.4*	4.0 ± 0.2*	3.4 ± 0.8*
	Plasmocytes	15.3 ± 1.6	21.8 ± 1.6*	19.3 ± 0.6*	33.5 ± 0.6*	14.7 ± 1.2	30.2 ± 0.2*	26.7 ± 0.8*
	Mastocytes	0.3 ± 0.01	0.8 ± 0.04*	0.4 ± 0.1	1.1 ± 0.1*	0.5 ± 0.1	1.0 ± 0.1*	0.8 ± 0.1*
	Mitotic figures	0.7 ± 0.1	1.9 ± 0.1*	1.4 ± 0.3*	1.2 ± 0.4*	0.6 ± 0.1	0.9 ± 0.1	0.9 ± 0.2

Note: M is arithmetic mean (M) and σ is the standard deviation; * is p calculated relative to the control group ($P < 0.05$). Counting of cell elements of mesenteric lymph nodes were carried out in the various functional areas of the lymph node with magnification ×1000 in 10 fields of view on the conventional unit area (6400 μm^2).

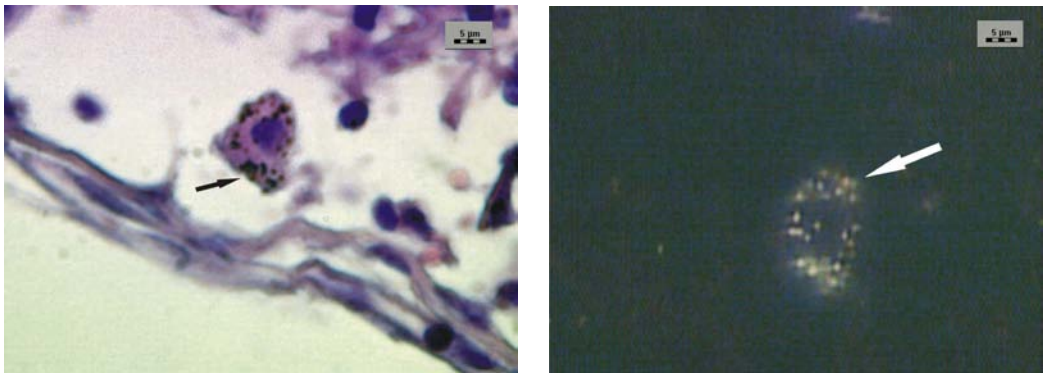

(a) (b)

Fig. 5. (a) Conglomerates of 50 nm GNPs in the cytoplasm of macrophage in cortex of lymph node. H-E staining, magnification 1500.0×. (b) Glow of 50 nm GNPs due to intensive light scattering. The arrow demonstrate conglomerates of 50 nm GNPs in the cytoplasm of macrophage. Dark-field microscopy, magnification 1500.0×.

In work[32] on melanoma-bearing mouse model the real-time lymphatic mapping and detecting metastasis in sentinel lymph nodes were done using 30 nm spherical polyethylene glycol (PEG) coated magnetic nanoparticles and golden carbon nanotubes as contrast agents for noninvasive photoacoustic techniques. The detection and photothermal treatment of nonpigmented breast cancer cells in sentinel lymph nodes were achieved by previous labeling them with nanoparticles. In this study and in recent work,[33] the enhancement of imaging depth in lymph nodes were demonstrated by using of optical clearing techniques.

Previously, we demonstrated that after single and repeated intraperitoneal administration of magnetite nanoparticles, their assemblages have been found at sites of injections and in lymph nodes of abdominal cavity.[34] Under continuous administration, the accumulation of nanoparticles is so pronounced that lymph nodes showed up contrasted on MRI.

In this study, we showed that prolonged peroral administration caused accumulation of GNPs in mesenteric lymph nodes. In the future research, it may be used for hyperthermia of mesenteric lymph nodes containing tumor cells (metastasis), and abdominal carcinomatosis.

5. Conclusions

In this work, we have studied the morphological changes in internal organs after a prolonged oral administration of GNPs. The main idea of the present study was to evaluate the reversibility of alterations noticed in internal organs of animals exposed to GNPs of different size. In particular, 2 nm, 15 nm, and 50 nm GNPs were administered for 1 mL of GNPs once a day for 30 days at a dosage of 190 μg/kg of body weight and the reversibility of morphological changes was assessed 14 days after the end of 30-days oral administration of GNPs. The main results of the study are as follows.

After the prolonged administration of GNPs, the severity of morphological changes in the liver, kidney, spleen and lymph nodes depended on the GNP size. In the liver and kidneys, the administration of GNPs led mainly to the development of venous hyperemia and edema as well as dystrophic and necrobiotic processes of varying severity. In the liver, spleen and lymph nodes, the activation of proliferation and differentiation of immune cells and macrophages was observed. The 50 nm GNPs caused the most pronounced dystrophic and necrobiotic processes, and 2 nm GNPs caused proliferative changes. The development of pathological processes was reversible, as evidenced by the restoration of the organ structure at 14 days after the end of GNP administration, the degree of reversibility depended on the size of the GNPs.

Thus, the reversibility of morphological changes in internal organs after prolonged peroral administration of GNPs indicates a low level of GNP toxicity at large time scale. Accordingly, GNP can be recommended for application to diagnostic and therapeutic treatment including *in vivo* noninvasive detection and treatment of metastases in sentinel lymph nodes.

Acknowledgments

This study was supported by Grant No. 14-13-01167 from the Russian Scientific Foundation. The morphological studies done by GNM, SSP, OVZ, IOB and NAN were conducted by the state task of Russian ministry of Health. The work done by VVT on interpretation of experimental data was supported by Grant No. 14-15-00186 of the Russian Science Foundation.

References

1. V. Torchilin, *Handbook of Nanobiomedical Research. Fundamentals, Applications and Recent Developments* (In 4 Volumes), World Scientific, Singapore (2014).
2. M. Valcárcel, Á. I. López-Lorente, *Gold Nanoparticles in Analytical Chemistry*, Elsevier, Amsterdam (2014).
3. E. Boisselier, D. Astruc, "Gold nanoparticles in nanomedicine: Preparations, imaging, diagnostics, therapies and toxicity," *Chem. Rev.* **38**, 1759–1782 (2009).
4. L. A. Dykman, N. G. Khlebtsov, "Gold nanoparticles in biomedical applications: Recent advances and perspectives," *Chem. Soc. Rev.* **41**, 2256–2282 (2012).
5. E. C. Dreaden, A. M. Alkilany, X. Huang, C. J. Murphy, M. A. El-Sayed, "The golden age: Gold nanoparticles for biomedicine," *Chem. Soc. Rev.* **41**, 2740–2779 (2012).
6. N. G. Khlebtsov, L. A. Dykman, "Biodistribution and toxicity of engineered gold nanoparticles: A review of *in vitro* and *in vivo* studies," *Chem. Soc. Rev.* **40**, 1647–1671 (2011).
7. M. I. Stockman, "Nanoplasmonics: Past, present, and glimpse into future," *Opt. Express* **19**, 22029–22106 (2011).
8. N. G. Khlebtsov, L. A. Dykman, "Optical properties and biomedical applications of plasmonic nanoparticles," *J. Quant. Spectr. Radiat. Transfer* **111**, 1–35 (2010).
9. M. A. Dobrovolskaia, S. E. McNeil, "Immunological properties of engineered nanomaterials," *Nat. Nanotechnol.* **2**, 469–478 (2007).
10. P. C. Chen, S. C. Mwakwari, A. K. Oyelere, "Gold nanoparticles: From nanomedicine to nanosensing," *Nanotechnol. Sci. Appl.* **1**, 45–66 (2008).
11. G. E. Abraham, "Clinical applications of gold and silver nanocolloids," *Original Internist* **15**, 132–158 (2008).
12. H.-J. Yen, S.-H. Hsu, Ch.-L. Tsai, "Cytotoxicity and immunological response of gold and silver nanoparticles of different sizes," *Small* **5**, 1553–1561 (2009).
13. P. R. Gil, G. Oberdörster, A. Elder, V. Puntes, W. J. Parak, "Correlating physico-chemical with toxicological properties of nanoparticles: The present and the future," *ACS Nano* **4**, 5527–5531 (2010).
14. A. M. Alkilany, C. J. Murphy, "Toxicity and cellular uptake of gold nanoparticles: What we have learned so far?," *Nanopart. Res.* **12**, 2313–2333 (2010).
15. I. M. Paino, V. S. Marangoni, R. de Cássia Silva de Oliveira, L. M. G. Antunes, V. Zucolotto, "Cyto- and genotoxicity of gold nanoparticles in human hepatocellular carcinoma and peripheral blood mononuclear cells," *Toxicol. Lett.* **215**, 1191–1125 (2012).
16. M. Schulz, L. Ma-Hock, S. Brill, V. Strauss, S. Treumann, S. Gröters, B. van Ravenzwaay, R. Landsiedel, "Investigation on the genotoxicity of different sizes of gold nanoparticles administered to the lungs of rats," *Mutat. Res.* **745**, 51–57 (2012).
17. S. Di Bucchianico, M. R. Fabrizi, S. Cirillo, C. Uboldi, D. Gilliland, E. Valsami-Jones, L. Migliore, "Aneuploidogenic effects and DNA oxidation induced *in vitro* by differently sized gold nanoparticles," *Int. J. Nanomed.* **9**, 2191–2204 (2014).
18. S. Fraga, H. Faria, M. E. Soares, J. A. Duarte, L. Soares, E. Pereira, C. Costa-Pereira, J. P. Teixeira, M. de Lourdes Bastos, H. Carmo, "Influence of the surface coating on the cytotoxicity, genotoxicity and uptake of gold nanoparticles in human HepG2 cells," *J. Appl. Toxicol.* **10**, 1111–1119 (2013).
19. H. Yang, C. Sun, Z. Fan, X. Tian, L. Yan, L. Du, Y. Liu, C. Chen, X.-J. Liang, G. J. Anderson, J. A. Keelan, Y. Zhao, G. Nie, "Effects of gestational age and surface modification on materno-fetal transfer of nanoparticles in murine pregnancy," *Sci. Rep.* **2**, 847 (2012).
20. X. Tian, M. Zhu, L. Du, J. Wang, Z. Fan, J. Liu, Y. Zhao, G. Nie, "Intrauterine inflammation increases materno-fetal transfer of gold nanoparticles in a size-dependent manner in murine pregnancy," *Small* **9**, 2432–2439 (2013).
21. N. A. Tsyganova, R. M. Khairullin, G. S. Terentyuk, B. N. Khlebtsov, V. A. Bogatyrev, L. A. Dykman, S. N. Erykov, N. G. Khlebtsov, "Penetration of pegylated gold nanoparticles through rat placental barrier," *Bull. Exp. Biol. Med.* **157**, 383–389 (2014).
22. L. A. Dykman, N. G. Khlebtsov, "Uptake of engineered gold nanoparticles into mammalian cells," *Chem. Rev.* **114**, 1258–1288 (2014).
23. J. F. Hillyer, R. M. Albrecht, "Gastrointestinal persorption and tissue distribution of differently

sized colloidal gold nanoparticles," *J. Pharm. Sci.* **90**, 1927–1936 (2001).

24. T. Jung, W. Kamm, A. Breitenbach, E. Kaiserling, J. X. Xiao, T. Kissel, "Biodegradable nanoparticles for oral delivery of peptides: Is there a role for polymers to affect mucosal uptake?," *Eur. J. Pharm. Biopharm.* **50**, 147–160 (2000).
25. L. A. Dykman, V. A. Bogatyrev, S. Y. Shchegolev, N. G. Khlebtsov, *Gold Nanoparticles: Synthesis, Properties, Biomedical Applications*, Nauka, Moscow (2008) (in Russian).
26. G. Frens, "Controlled nucleation for the regulation of the particle size in monodisperse gold suspensions," *Nat. Phys. Sci.* **241**, 20–22 (1973).
27. D. G. Duff, A. Baiker, P. P. Edwards, "A new hydrosol of gold clusters. 1. *Formation and Particle Size Variatio*," *Langmuir* **9**, 2301–2309 (1993).
28. G. A. Merkulov, The Course of Patohistologic Technology, Medicine, Leningrad (1969) (in Russian).
29. International Guiding Principles for Biomedical Research Involving Animals, CIOMS&ICLAS, http://www.cioms.ch/index.php/12-newsflash/227-cioms-and-iclas-release-the-new-international-guiding-principles-for-biomedical-research-involving-animals (2012).
30. I. M. Solopaeva, B. P. Solopaev, Stimulation of regeneration of the diseased liver and human chorionic gonadotropin, Nizhny Novgorod, Univ N. I. Lobachevsky (1991).
31. V. V. Sadovnikova, I. V. Sadovnikova, L. N. Ivanova, "Morphological changes in the liver of rats with drug-induced hepatitis and toxic stimulation of reparative processes," *Morphology* **120**, 63–65 (2001).
32. E. I. Galanzha, M. S. Kokoska, E. V. Shashkov, J. W. Kim, V. V. Tuchin, V. P. Zharov, "*In vivo* fiber-based multicolor photoacoustic detection and photothermal purging of metastasis in sentinel lymph nodes targeted by nanoparticles," *J. Biophoton.* **2**, 528–539 (2009).
33. E. Song, H. Seo, K. Choe, Y. Hwang, J. Ahn, S. Ahn, P. Kim, "Optical clearing based cellular-level 3D visualization of intact lymph node cortex," *Biomed. Opt. Express* **6**, (2015). doi: 10.1364/BOE.6.004154.
34. S. V. German, O. A. Inozemtseva, N. A. Navolokin, E. E. Pudovkina, V. V. Zuev, E. K. Volkova, A. B. Bucharskaya, S. N. Pleskova, G. N. Maslyakova, D. A. Gorin, "Synthesis of magnetite hydrosols and assessment of their impact on living systems at the cellular and tissue levels using MRI and morphological investigation," *Nanotechnol. Russia* **8**, 573–580 (2013).